Single-phase catalysis for reductive etherification of diesel bioblendstocks

Journal:	*Green Chemistry*
Manuscript ID	GC-ART-03-2020-000939.R1
Article Type:	Paper
Date Submitted by the Author:	12-May-2020
Complete List of Authors:	Hafenstine, Glenn; National Renewable Energy Laboratory, National Bioenergy Center Huq, Nabila; National Renewable Energy Laboratory Conklin, Davis; National Renewable Energy Laboratory, National Bioenergy Center Wiatrowski, Matthew; National Renewable Energy Laboratory, National Bioenergy Center Huo, Xiangchen; National Renewable Energy Laboratory, National Bioenergy Center Guo, Qianying; Oak Ridge National Laboratory, Materials Science and Technology Division Unocic, Kinga; Oak Ridge National Laboratory, Materials Science and Technology Division Vardon, Derek; National Renewable Energy Laboratory, National Bioenergy Center

Single-phase catalysis for reductive etherification of diesel bioblendstocks

Glenn R. Hafenstine, [a] Nabila A. Huq, [a] Davis R. Conklin, [a] Matthew R. Wiatrowski, [a] Xiangchen Huo, [a] Qianying Guo, [b] Kinga A. Unocic, [b] and Derek R. Vardon [a]*

Reductive etherification is a promising catalytic chemistry for coupling biomass derived alcohols and ketones to produce branched ethers that can be used as high cetane, low sooting blendstocks for diesel fuel applications. Previous catalyst materials examined for reductive etherification have typically been limited to binary physical mixtures of metal hydrogenation and acidic acetalization catalysts with limited thermal stability and industrial applicability. To address this, we developed a single-phase catalyst comprised of Pd supported on acidic metal oxides with high catalytic activity, product selectivity, and regeneration stability. Batch reactor screening identified niobium phosphate ($NbOPO_4$) as the most active acidic metal oxide catalyst support, which was downselected to synthesize single-phase catalysts by Pd loading. Several branched ethers with favourable fuel properties were synthesized to demonstrate broad catalyst applicability. The fresh $Pd/NbOPO_4$ catalyst displayed a surface area of 130 m^2 g^{-1}, high acidity of 324 μmol g^{-1} and Pd dispersion of 7.8%. The use of acidic metal oxide support allowed for elevated reaction temperatures with a mass selectivity to 4-butoxyheptane of 81% at 190 °C and an apparent activation energy of 40 kJ mol^{-1}. Continuous flow reactor testing demonstrated steady catalyst deactivation due to coke formation of 10 wt% after 117 h of time-on-stream. Four simulated catalyst regeneration cycles led to small changes in surface area and total acidity; however, a decrease in Pd site density from 18 to 8 μmol g^{-1}, in combination with an apparent Pd nanoparticle size effect, caused an increase in the production rate of 4-butoxyheptane from 138 to 190 μmol g_{cat}^{-1} min^{-1} with the regenerated catalyst. Lastly, technoeconomic analysis showed that higher H_2 equivalents and lower weight hourly space velocity values can reduce ether catalytic production costs.

Introduction

Sustainable pathways are needed to produce renewable fuels for diesel applications, despite the growth of electrification for light duty vehicles.[1] Sustainable fuels must overcome technical and market hurdles in order to achieve wide-spread adoption, which include competitive production costs, process de-risking, infrastructure compatibility, and suitable fuel properties with minimal emissions.[2] Oxygenated diesel bioblendstocks offer several advantages over hydrocarbon analogues when blended into conventional petroleum diesel. Biomass natively contains a considerable amount of oxygen (30–40 wt% of dry matter),[3] and hydrocarbon production from biomass typically requires extensive oxygen removal in the form of carbon dioxide or water. This results in significant hydrogen demand and overall mass loss, which impact process economics.[4] From a fuel property standpoint, a recent computational screening of >400 theoretically accessible bioblendstocks[5] for heavy-duty engine applications has shown

the advantage of targeting ethers to improve diesel fuel cetane number and lower the intrinsic sooting tendency (as quantified by yield sooting index).[6, 7]

Integrated biological and chemo-catalytic processing affords pathways to valuable biobased fuels and chemicals.[8-12] Previous work from our group identified 4-butoxyheptane (4-BH) as a promising branched ether diesel bioblendstock that displays excellent fuel properties and potential infrastructure compatibility.[13] Ether molecules such as 4-BH can be produced through reductive etherification, which couples specific alcohol and ketone intermediates. These intermediates can be produced from biomass through several routes including fermentation of sugars,[14, 15] catalytic carbohydrate conversion,[16] oxidation of branched alcohols[17-19] and conversion of waste-derived volatile fatty acids[20-22] (**Scheme 1**). As such, reductive etherification offers significant flexibility to upgrade diverse acid, alcohol and ketone substrates into an ether bioblendstock that can help lower separation costs and increase the overall process carbon balance.[23, 24]

a. *National Renewable Energy Laboratory, 15013 Denver West Parkway, Golden, CO, USA. E-mail: Derek.Vardon@nrel.gov*
b. *Oak Ridge National Laboratory, 1 Bethel Valley Road, Oak Ridge, TN, USA.*
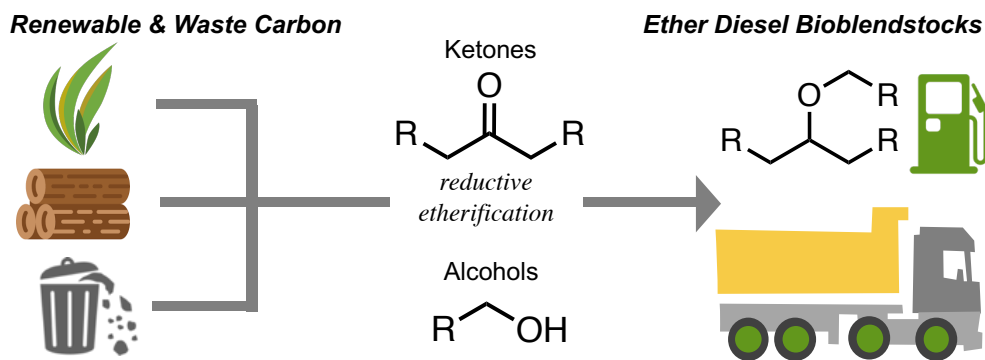
Scheme 1: Production of renewable diesel bioblendstocks through reductive etherification of alcohols and ketones.

Coupling of the alcohol and ketone intermediates through reductive etherification is feasible using a physical mixture of supported palladium catalyst for hydrogenation chemistry, alongside solid acid catalyst for ketalization and dehydration chemistry. As shown in **Scheme 2**, reduction of carbonyl compounds with subsequent alcohol etherification has been demonstrated over various metal catalysts,[25-28] but reactivity of 2° alcohols such as 4-heptanol is dominated by dehydration over etherification.[29, 30] Lemaire *et al.* first demonstrated reductive etherification through a tandem acetalization and hydrogenation pathway over mixed catalysts of palladium and solid acid as an alternative for reductive etherification of sterically hindered carbonyl reactants.[31] Several subsequent papers have shown reductive etherification through ketal or enol ether intermediates over palladium and acid catalyst mixtures[32-36] with only ketalization products forming over acid in the absence of a precious metal catalyst.[36-38] One notable exception from Bell *et al.* demonstrated the formation of acetal compounds during ether-producing reactions using a PtSn alloy instead of Pd metal.[38]

While numerous studies have demonstrated this reaction under a range of temperatures and hydrogen pressures, less work has focused on developing continuous, solvent-free catalytic processes relevant to industrial adoption and the twelve principles of green chemistry.[39] While our previous work on continuous production of 4-BH[13] was promising, the catalyst mixtures showed a steady decline in activity over 89-hour runs. Deactivation of acidic catalyst materials frequently occurs due to water adsorption onto Brønsted acid sites[40] or carbon laydown onto the surface as coke.[41] While water removal can be performed under inert gas flow, regenerating a coked catalyst requires both heat and oxygen which can lead to structural changes in activated carbon and polymer resin support materials.[42] In addition, the formation of water as a by-product of reductive etherification can over time degrade silica and alumina metal oxide catalyst supports that have been investigated for reductive etherification,[43 35-37, 44-47] motivating the use of hydrothermally stable metal oxides that provide sufficient acidity.[45, 47]

Therefore, in this work we downselected a catalyst for reductive etherification from several hydrothermally stable

support options with Pd deposition to form a single-phase material. Regenerability of the selected catalyst was demonstrated with *ex situ* thermal and oxidative cycling in coordination with characterization of active site density and batch reaction testing. The effect of Pd nanoparticle size on the kinetics and selectivity of reductive etherification was studied using scanning transmission electron microscopy (STEM) imaging. The utility of the single-phase catalyst was demonstrated by producing a range of ether bioblendstocks suitable for diesel applications. We also address the potential for process intensification by reducing downstream separation and recycle demands through catalyst design. Novel ether bioblendstock candidates were produced using batch reactor conditions to confirm the broad applicability of the catalyst with a variety of ketone and alcohol substrates. Advantageous diesel bioblendstock fuel properties were then validated from a range of unique ether molecules. Reductive etherification reaction conditions were optimized in a continuous production system to improve the selectivity for 4-butoxyheptane. Long-term catalyst performance and coke formation was demonstrated through >100-h time-on-stream tests. The cost of the single-
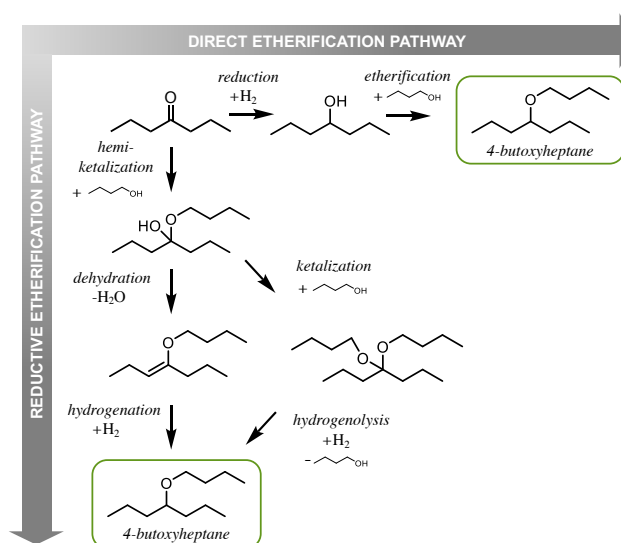
Scheme 2: Possible reaction pathways for the synthesis of 4-butoxyheptane through direct and reductive etherification.

phase catalyst material was estimated using the CatCost software and incorporated into a technoeconomic analysis (TEA) model for upgrading wet waste volatile fatty acids. Finally, the impact of improving ether yield and selectivity on process costs was evaluated in order to inform further research and development for single-phase catalyst design.

Results and discussion

Catalyst support synthesis

Acidic metal oxide catalyst supports based on niobia and titania were initially synthesized and screened to provide an alternative to acidic resins used for reductive etherification. These metal oxides are known to provide high total acidity, as well as increased resistance to structural change under hydrothermal conditions when compared to SiO_2 and Al_2O_3.[43, 49, 50] Our previous work explored the use of both Nb_2O_5 and ZrO_2,[13] and we examined the phosphated form of these catalysts to increase Brønsted acidity, which may be beneficial for the initial reaction steps of hemi-ketalization, ketalization and dehydration. Surface phosphating procedures with niobic acid (Nb_2O_5-PO_4) have previously been demonstrated as a viable alternative to Amberlyst-15.[13] Titanium dioxide was
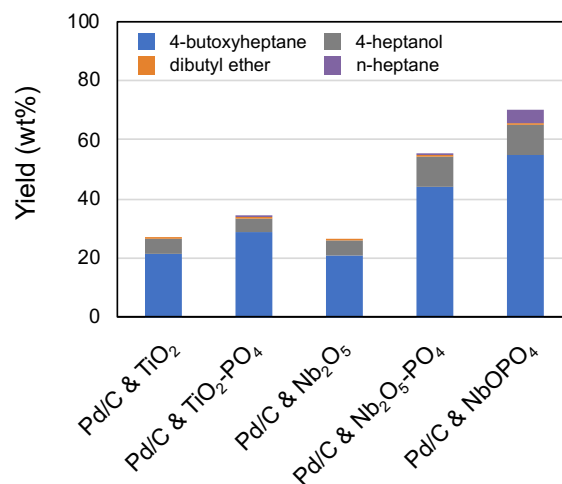

Figure 1: Acidic metal oxide support screening using Parr batch reactors. Batch conditions: 190 °C, 1000 psig H_2, 20 mL equimolar n-butanol/4-heptanone solution, 680 mg of acidic metal oxide support, 230 mg of Pd/C, 800 rpm, 1 h.

Table 1: Acidic metal oxide catalyst support material properties. *

Metal Oxide Support	Surface Area ($m^2 g^{-1}$)	Pore Vol ($cm^3 g^{-1}$)	Total Acidity ($\mu mol\ g^{-1}$)	Brønsted Lewis Ratio
Nb_2O_5-PO_4	71	0.09	124	0.30
Nb_2O_5	40	0.11	71	0.13
TiO_2-PO_4	134	0.38	274	0.12
TiO_2	107	0.36	215	0.00
$NbOPO_4$	136	0.28	269	0.80

* Metal oxide supports were initially calcined at 400 °C for 5 h in static air prior to characterization.

obtained from Alfa Aesar, and both Nb_2O_5 and $NbOPO_4$ were

obtained from CBMM. Catalyst supports were initially crushed, sieved, and calcined at 400 °C to before phosphating or testing catalytic performance.

Characterization of the acidic metal oxide supports (**Table 1**) determined higher surface area and acidity from the TiO_2 and $NbOPO_4$ base materials relative to Nb_2O_5. However, calcining niobic acid hydrate above 250 °C begins to increase the crystallinity of the material and subsequently decreases the surface area and acidity[51] with the non-calcined Nb_2O_5 having a total acidity of 361 $\mu mol\ g^{-1}$. The phosphating procedure increased the surface area, total acidity and Brønsted acidity of the Nb_2O_5 and TiO_2 base supports.

Next, acidic metal oxides were co-mixed with 5 wt% palladium-on-carbon (Pd/C) and screened for reductive etherification. 4-BH was the target ether compound produced in a multi-batch Parr reactor system under 1000 psig H_2, at 190

Table 2: Material properties of fresh, spent, and regenerated single-phase catalysts tested for reductive etherification. NP = nanoparticle.

Single Phase Catalyst	Surface Area ($m^2 g^{-1}$)	Pore Vol ($cm^3 g^{-1}$)	Total Acidity ($\mu mol\ g^{-1}$)	Pd Site Density ($\mu mol\ g^{-1}$)	CO Chemi Pd NP Diameter (nm)	Scherrer Pd NP Diameter (nm)	TEM Pd NP Diameter (nm)
Fresh Pd-Nb_2O_5-PO_4	57	0.12	120	16	16	13	N/A
Fresh Pd-TiO_2-PO_4	134	0.38	272	35	8	6	N/A
Fresh Pd-$NbOPO_4$	131 ± 2	0.28 ± 0.01	358 ± 48	16 ± 3	15 ± 1	10 ± 2	10 ± 9
117 h Spent Pd-$NbOPO_4$	99	0.24	274	2	145	N/A	9 ± 6
Regen 1x Pd-$NbOPO_4$	132	0.29	384	10	27	11	N/A
Regen 4x Pd-$NbOPO_4$	116	0.26	364	8	34	14	5 ± 6

* After Pd loading, single phase catalysts were initially calcined at 265 °C for 2 h and reduced at 265 °C for 5 h. Ether production rates were measured at conditions: 190 °C, 1000 psig H_2, 30 cm^3 (STP) min^{-1} H_2, 0.05 mL min^{-1} equimolar n-butanol/4-heptanone feed, 0.5 g catalyst. Catalyst regeneration cycles were performed by cycles of oxidation under zero air at 350 °C for 2 h and reduction under H_2 at 265 °C for 3 h with ramping steps performed under N_2 purge at 5 °C min^{-1}.

°C with 800 rpm stirring, 20 mL equimolar n-butanol/4-heptanone, 230 mg of Pd/C and 680 mg of metal oxide for 1 h. As shown in **Figure 1**, the yield of 4-BH trended as $Nb_2O_5 < TiO_2 < TiO_2-PO_4 < Nb_2O_5-PO_4 < NbOPO_4$ and the full quantification dataset from batch screening is provided in **Table S1**. This trend is not fully accounted for by differences in Brønsted or total acidity, suggesting the multi-step reaction pathway may employ catalysis on both Brønsted and Lewis acid sites with a complex effect on rate and equilibrium.

The proposed catalytic reaction pathway in **Scheme 2** was also supported through batch reactor tests that compared 4-heptanone reduction to direct etherification of n-butanol with 4-heptanol under identical reaction conditions (**Figure S4**). In the absence of an acid catalyst, trace amounts of 4-heptanol were formed (1 ± 0.2 wt%), suggesting that ketone-to-alcohol reduction is not the initial reaction step leading to 4-BH formation. Likewise, the direct etherification reaction between n-butanol and 4-heptanol to form 4-BH only yielded 1 ± 1 wt%. These results suggest that under the conditions tested, reductive etherification likely proceeds through the hemi-ketalization pathway (vertical reaction, **Scheme 2**), with the ketone reduction pathway (top horizontal reaction, **Scheme 2**) being significantly slower.

Single-phase catalyst development

Single-phase catalysts were then prepared using the suite of phosphated acidic metal oxide supports. Palladium was deposited through incipient wetness impregnation, which can form metal crystallites on the scale of several nanometers in diameter.[52] Strong electrostatic adsorption was also considered as a deposition method, since it has been shown to produce
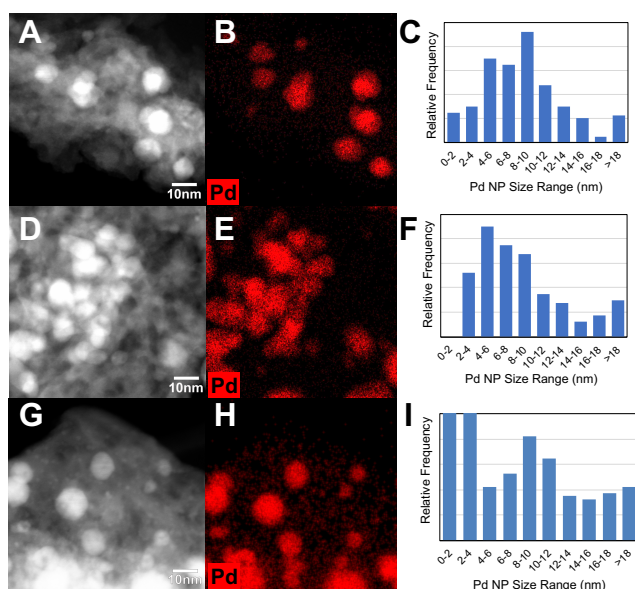
Figure 2: Characterization of $Pd/NbOPO_4$ by STEM-EDS. Samples include fresh catalyst (a, b, c), spent catalyst after 117 h time-on-stream (d, e, f), and regenerated catalyst after 4 simulated cycles (g, h, i). Histograms were prepared from analysis of >100 Pd NPs and the raw data can be found in **Table S2**.
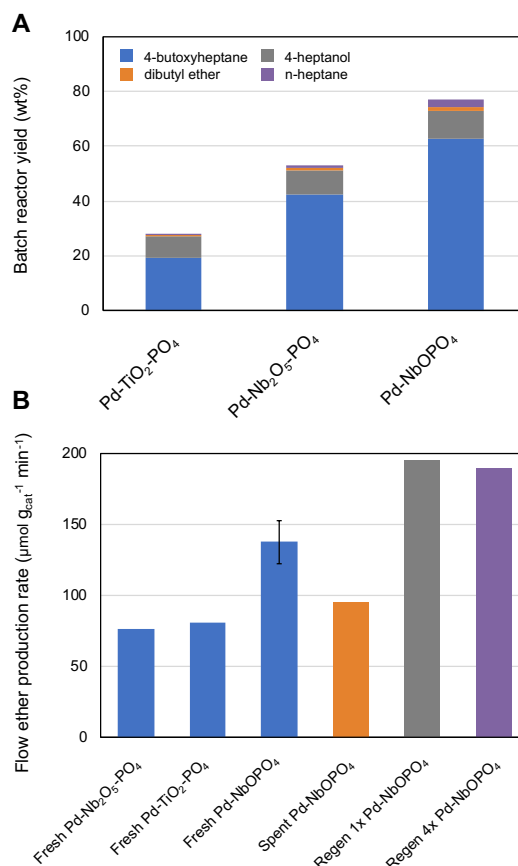
Figure 3: Single-phase catalyst batch reactor screening (a) and flow reactor testing (b). Batch conditions: 190 °C, 1000 psig H_2, 20 mL equimolar n-butanol/4-heptanone solution, 680 mg of single-phase catalyst, 800 rpm, 1 h. Flow conditions: 190 °C, 1000 psig H_2, 30 cm³ (STP) min⁻¹ H_2, 0.05 mL min⁻¹ equimolar n-butanol/4-heptanone feed, 0.5 g catalyst (WHSV 4.9 h⁻¹). Simulated regeneration conditions: 4 cycles of oxidation under zero air at 350 °C for 2 h, followed by reduction under 200 cm³ (STP) min⁻¹ H_2 at 265 °C for 3 h with ramping steps performed under N_2 purge at 5 °C min⁻¹.

smaller nanoparticles leading to increased utilization of precious metal per unit mass.[53] However, minimizing Pd crystal size is not necessarily optimal for reductive etherification based upon previous studies.[36, 47] Corma *et al.* recently demonstrated an optimal Pd crystallite diameter of 10 nm for the coupling of n-octanol with methyl levulinate.[47] Marecot *et al.* also showed an increased rate of ether formation on crystals of 18 nm in diameter compared to 10 nm in diameter.[36] Based upon these results, we focused on the use of incipient wetness for Pd deposition.

Single-phase catalysts were then prepared with 5 wt% Pd to determine the effect of metal loading on material properties (**Table 2**). The loading of Pd on metal oxide was chosen to achieve similar conversion values to the Pd/C mixtures in the batch reaction screening tests. Minor changes in surface area and total acidity were seen for all catalysts after metal loading. CO chemisorption showed that Pd/TiO_2-PO_4 had approximately double the number of accessible Pd sites (35 µmol g⁻¹) relative to the niobium support materials (16 µmol g⁻¹) (see **Figure S3** for CO pulse traces). Pd metal crystallite sizes from XRD and

Scherer analysis showed the same trend of increasing size from Pd/TiO$_2$-PO$_4$<Pd/NbOPO$_4$<Pd/Nb$_2$O$_5$-PO$_4$. However, STEM imaging of Pd/NbOPO$_4$ (**Figure 2a,b**) suggests a more complex mixture of particle sizes with the as-synthesized material having an average particle size of 10 nm and a broad standard deviation of 9 nm (**Figure 2c, Table S2**).

The three single-phase catalysts were then evaluated to compare 4-BH yields and selectivity under batch and flow reactor conditions. In batch (**Figure 3a**), similar selectivity to 4-BH was seen for both Pd/TiO$_2$-PO$_4$ and Pd/Nb$_2$O$_5$-PO$_4$ relative to the binary physical mixtures of metal oxide and Pd/C, albeit with slightly lower conversion. Pd/NbOPO$_4$ was the highest yielding catalyst for 4-BH, with comparable selectivity. This may be due to the larger Pd metal crystallite sizes or higher total acidity. In flow reactor tests at ~30% molar 4-heptanone conversion (**Figure 3b**), Pd/NbOPO$_4$ also displayed a significantly higher ether production rate of 138 ± 15 µmol g$_{cat}^{-1}$ min^{-1}, when compared Pd/Nb$_2$O$_5$-PO$_4$ and Pd/TiO$_2$-PO$_4$ which ranged from 76 to 81 µmol g$_{cat}^{-1}$ min^{-1}, respectively. Interestingly, Pd/Nb$_2$O$_5$-PO$_4$ showed lower activity than Pd/TiO$_2$-PO$_4$ at low conversion in flow when compared to batch results. Based on these findings, Pd/NbOPO$_4$ was selected for further study.

Varied ether bioblendstock targets

The broad applicability of Pd/NbOPO$_4$ to produce ether diesel bioblendstocks was then demonstrated with a range of alcohols (C2-C8) and ketones (C3-C11). Target ether yields ranged from 40-70 wt% and mass selectivity was above 80% for all ethers apart from 1-isopropoxybutane (53%), as shown in **Figure 4**. The low selectivity to 1-isopropoxybutane may be due to high reactivity of acetone under these conditions. Additional quantification data and mass spectrometry with predicted and
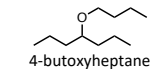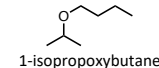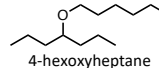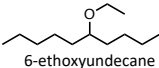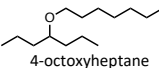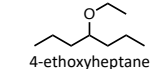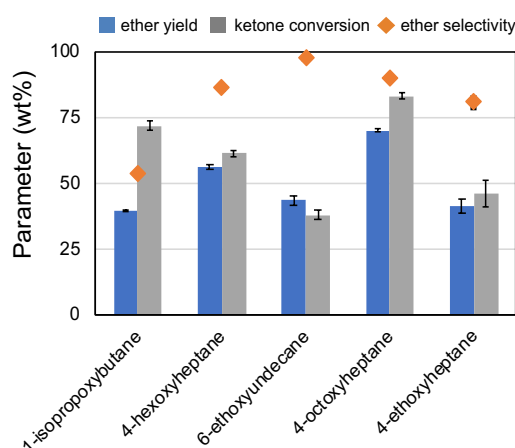
Figure 4: Application of Pd/NbOPO$_4$ to produce a variety of branched ether compounds via reductive etherification, with relevant diesel bioblendstock fuel properties provided in **Table 3**. Batch conditions: 190 °C, 1000 psig H$_2$, 20 mL equimolar solution, 680 mg of Pd/NbOPO$_4$, 800 rpm, 1 h. Products were analysed using GC/MS with fragmentation patterns matched to the NIST database or predicted using ChemDraw (**Figure S6**).

actual fragmentation patterns for atypical products are provided in **Table S3** and **Figure S6**, respectively.

Fuel properties of the novel ether bioblendstocks were then evaluated using predictive and experimental tools.[4, 13] Fuel property predictions alleviated the need for separation and purification of product reaction mixtures, as well as sample volume requirements required with traditional measurement techniques. Select fuel property measurements were provided in **Table 3** for reference. Bioblendstock fuel properties of interest included cetane number,[54, 55] and yield sooting index,[56,

Table 3: Measured and predicted fuel properties (latter in parentheses) for ether bioblendstocks. Fuel property criteria denotes desired values for existing U.S. diesel fuel infrastructure compatibility and safety requirements. Conventional base diesel was clay treated to remove additives. Base diesel and 4-BH values were previously reported.[3, 6]

	Cetane Number	Yield Sooting Index	Lower Heating Value (MJ kg^{-1})	Melting Point (°C)	Flashpoint (°C)	Boiling Point (°C)
Conventional base diesel *	44	215	43	-10	61	333
Target oxygenate blendstock properties	> 40	< 200	> 25	< 0	> 52	< 338
4-butoxyheptane	80 (76)	58 (55)	39 (40)	<-80 (-53)	64 (60)	198 (195)
1-isopropoxybutane	(76)	(24)	(38)	(-74)	(1)	(107)
4-hexoxyheptane	(71)	75 (78)	43 (41)	<-80 (-4)	68 (83)	234 (233)
6-ethoxyundecane	(74)	70 (78)	42 (41)	10 (-4)	83 (82)	236 (233)
4-octoxyheptane	(81)	(92)	(41)	(18)	(106)	(268)
4-ethoxyheptane	(63)	(35)	(39)	-68 (-50)	(31)	(152)

[57] as discussed previously; as well as lower heating value (LHV),[58-60] melting point,[61, 62] flash point,[63, 64] and boiling point.[61] Certain property criteria, such as melting and boiling point, are useful to ensure consistent phase behaviour in the engine environment in order to facilitate efficient fuel utilization. The melting point of the diesel fuel must be below 0 °C to prevent the fuel from freezing in cold weather, and the boiling point must stay below 338 °C so it can be vaporized. These metrics can be in opposition and require an optimization of blendstock candidate molecular structure and carbon number. The minimum flashpoint criterion of 52 °C ensures safe handling with respect to flammability. Finally, a high LHV indicates an energy dense fuel, which has positive implications for diesel fuel tank mileage.

All ether bioblendstocks displayed predicted cetane numbers ranging from 63-81, which is >40% above the base petroleum diesel value of 44 and advantageous when blending into low cetane fuels. Likewise, yield sooting index values ranged from 24-78, which is >60% below the base diesel value of 215. Lower heating values ranged from 38-43 MJ kg^{-1} due to the aliphatic chains and total carbon numbers that ranged from C7-C15. Although ether energy density values were lower than the base diesel, they all fell within 12%. The branched ether backbone facilitated melting points below freezing when the backbone was below C15; however, it should be noted that melting is notoriously difficult to predict,[62] and further experimental tests are needed to confirm predicted values. Lastly, C11 and above ethers passed the flashpoint cut-off for flammability, while the C7 and C9 ethers did not, which would limit their blend level in diesel.

Continuous performance and regeneration of Pd/NbOPO$_4$

Further testing of Pd/NbOPO$_4$ was performed in a trickle bed reactor to assess its temperature dependence for reductive etherification, as well as time-on-stream stability. Tests were performed at 190 °C and 1000 psig H$_2$ with 30 cm^3 (STP) min^{-1} of gas flowrate, 0.05 mL min^{-1} of equimolar 4-heptanone and n-butanol feed, and 0.5 g of catalyst. Pd/NbOPO$_4$ production rates and selectivity for 4-BH were measured at four reaction temperatures and 4-heptanone molar conversion below 50% after 17 h time-on-stream, with results shown in **Figure 5a**. An apparent activation energy of 40.0 kJ mol^{-1} for the three-step reaction was calculated. The reduced selectivity to 4-BH formation at 200 °C and 125 °C suggests a local maximum is present. While polymeric resins containing sulfuric acid functionalities are commonly used as acid catalysts due to their high Brønsted acidity, their lack of thermal stability (120 °C maximum for Amberlyst-15) prevents operation at the temperatures examined here.

Pd/NbOPO$_4$ stability was then evaluated under partial conversion conditions (36% molar conversion of 4-heptanone) for over 100 h of time on stream. As shown in **Figure 5b**, a steady decline in 4-BH production rate from 138 to 95 μmol g$_{cat}^{-1}$ min^{-1} was seen over the course of the 117-h test. The deactivation was attributed to carbon laydown, which was measured to be 10 wt% of the spent catalyst after reaction by
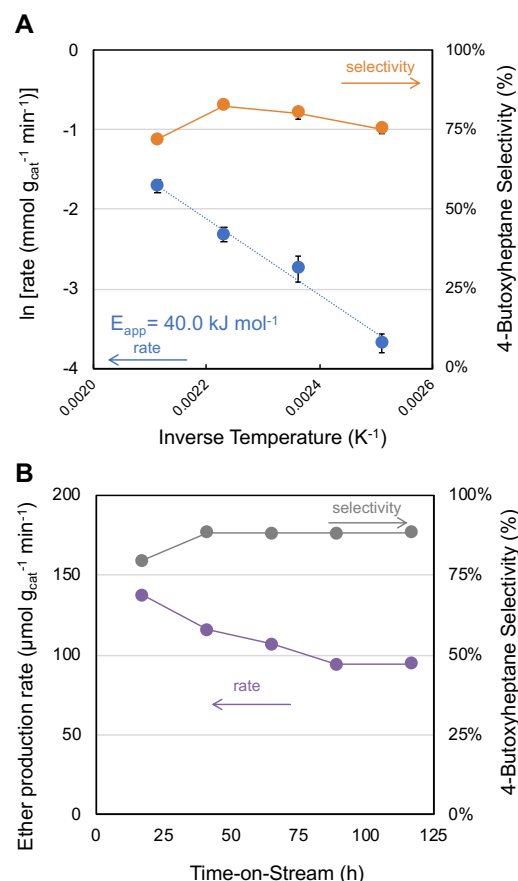

Figure 5: Initial rate of 4-BH formation and 4-BH selectivity vs. temperature with the apparent activation energy noted (a). Time-on-stream evaluation of 4-BH production rate and selectivity (b). Flow conditions: 125- 200 °C, 1000 psig H$_2$, 30 cm^3 (STP) min^{-1} H$_2$, 0.05 mL min^{-1} equimolar n-butanol/4-heptanone feed, 0.5 g Pd/NbOPO$_4$.

thermal gravimetric analysis-Fourier transform infrared spectroscopy (TGA-FTIR) (**Figure S7**). However, the selectivity to 4-BH increased to 88 % after an initial start-up value of 79 % due to a sharp drop in 4-heptanol and heptane formation, which may be due to carbon laydown blocking acidic dehydration sites and metallic Pd hydrogenation sites. Corresponding drops in surface area, total acidity and Pd site density were also observed in the spent catalyst (**Table 2**).

Reactor effluents at 33 h were analysed for Pd leaching due to the detrimental effect on catalyst lifetime and process economics.[65] Tests showed promising sub-ppm levels of Pd leaching levels, with 19 ppb for Pd/NbOPO$_4$, 8 ppb for Pd/Nb$_2$O$_5$-PO$_4$, and below detection limit of ~6 ppb for Pd/TiO$_2$-PO$_4$. Phosphorus leaching for Pd/NbOPO$_4$ was also tested by Southwest Research Institute using ASTM D3231 due to concerns of corrosion with engine metal components.[5] Results showed 0.38 ppm P in the effluent, which is far below the 10 ppm limit of B100 biodiesel.[66] STEM imaging of the spent catalysts showed little change in Pd NP sizes after 117 h of time on stream, with a decrease in average Pd particle size from 10 ± 9 nm to 9 ± 6 nm for the 117-h sample, as seen in **Figure 2d,e,f**.

Catalyst regeneration was evaluated by cycling reduction and oxidation at elevated temperatures to determine the impact on material properties and reductive etherification performance. As-synthesized Pd/NbOPO$_4$ was treated with either 1 or 4 cycles of oxidation under zero air at 350 °C and reduction under H$_2$ at 265 °C (detailed procedure included in the Supporting Information). At this temperature, 92% of the carbon had been removed from the spent catalyst during TGA-FTIR. As shown in **Table 1**, negligible changes in surface area and total acidity of the NbOPO$_4$ support occurred after regeneration. However, Pd surface area from CO chemisorption measurements decreased substantially after regeneration, suggesting Pd sintering. While the Scherrer crystallite size measurement from XRD spectra showed small increases in Pd nanoparticle size, STEM imaging revealed a more complex distribution. The regenerated samples showed a sharp increase in the number of small Pd crystals (<4 nm), with an average size of 5 ± 6 nm (**Figure 2g,h,i**). The number of larger Pd NPs remained fairly constant however which accounts for the small changes in XRD and CO chemisorption results. Interestingly, the regenerated catalyst displayed the highest ether production rates of 195 µmol g$_{cat}^{-1}$ min^{-1} despite the drop in Pd dispersion, which remained stable after 4-regeneration cycles (190 µmol g$_{cat}^{-1}$ min^{-1}), as shown in **Figure 3b**. Previous studies have shown a strong dependence on reductive ether yields with increasing Pd nanoparticle sizes above 10 nm.[36, 47] Further work is needed to understand the mechanism governing the reaction rate to guide future catalyst material design and regeneration protocols.

Reductive etherification process economics

Technoeconomic modelling was performed to explore the relationship between catalytic process conditions, reductive etherification performance, catalyst material costs, and downstream separations. Outputs are reported in regard to the minimum fuel selling price (MFSP) of ether bioblendstock on a gallon of gasoline equivalent basis ($/GGE). Emphasis is given to observing the net change in MFSP over a range of different process parameters relating to the reductive etherification unit operation (see **Figure 6a**), rather than the overall MFSP. For reductive etherification, a catalyst lifetime of 2 years was assumed with the operation of parallel reactors for periodic regeneration. Using the recently developed CatCost software for catalyst price estimation,[67,68] cost of the single-phase Pd/NbPO4 catalyst was estimated to be $406 kg^{-1}, with the primary cost driver being 5 wt% Pd loading (~81%).

To model the production of butyric acid as the key intermediate, our previous work explored the biochemical conversion of corn stover.[13] Here, we have elected to analyse an upstream process to produce butyric acid from the anaerobic digestion of wastewater sludge on a scale of 300 dry tonnes per day to significantly lower feedstock cost (asserted to be delivered in this case at no cost to the plant, which would be co-located with an existing wastewater treatment plant) and alleviate the need for biobased chemical co-products.[48] However, it should be noted that there are several
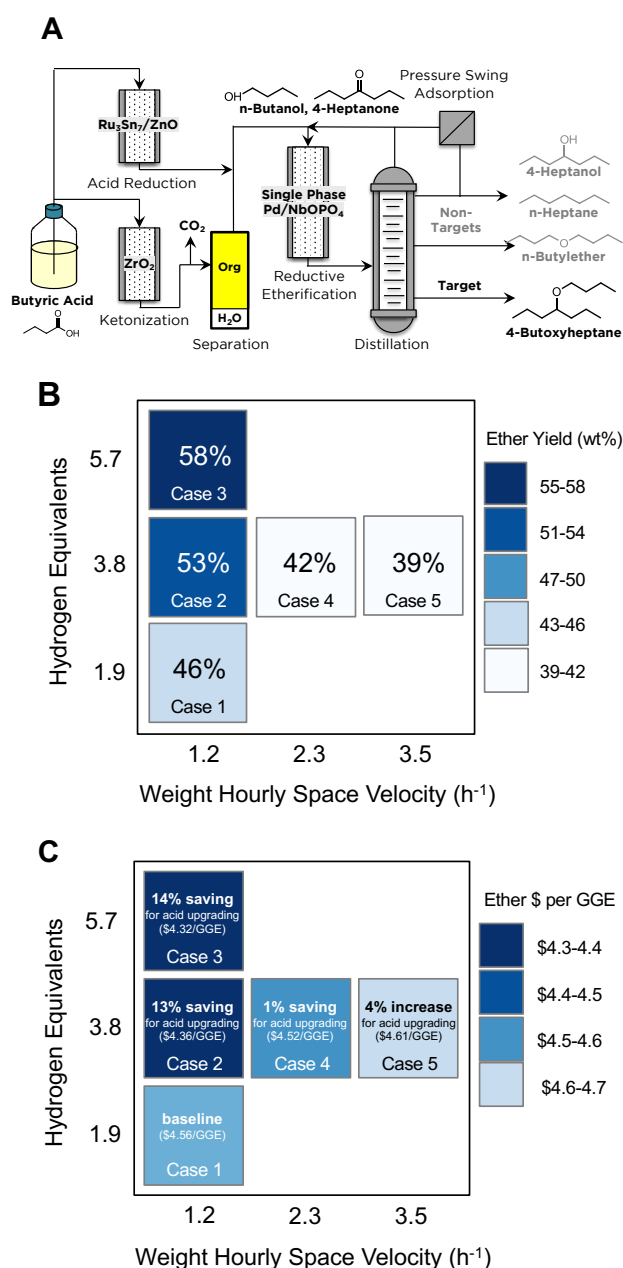

Figure 6: Process flow diagram for upgrading butyric acid to 4-BH (a), continuous flow reactor results showing 4-BH yield vs. H$_2$ flow equivalents and WHSV at conditions: 190 °C, 1000 psig H$_2$, 8-50 cm^3 (STP) min^{-1} H$_2$, 0.05-0.15 mL min^{-1} equimolar n-butanol/4-heptanone feed, 2.1 g Pd/NbOPO$_4$ single-phase catalyst (b) and minimum fuel selling price ($/GGE) vs WHSV and H$_2$ equivalents (c).

technological hurdles that must be overcome before a commercial scale *n-th* plant could be established. Specifically, the model asserts to produce pure butyric acid from anaerobic digestion; though selective propanoic or butyric acid production has been shown experimentally with lignocellulosic biomass,[69-71] a more diverse feedstock such as wastewater sludge presents additional challenges.[23,24] Additionally, the recovery of the acid from the anaerobic digestion occurs via pertractive membrane; a technology that has shown great promise but that has not

been demonstrated thus far at a large scale.[72] As noted above, the scope of this analysis is to analyse the impact of reductive etherification parameters of interest, namely, H_2 equivalency and catalyst WHSV. Additional details and references about the TEA model can be found in the Supplementary Information.

A range of stoichiometric equivalents of H_2 flow and liquid weight-hourly space velocity (WHSV) values were examined experimentally to determine the impact on 4-BH yield and selectivity. Tests were performed at the following conditions: 190 °C, 1000 psig H_2, 1.9-5.7 stoichiometric equivalents of H_2 flow, 0.05-0.15 mL min^{-1} of equimolar 4-heptanone and n-butanol feed (corresponding to WHSV ranging from 1.2-3.5 h^{-1}), and 2.1 g of Pd/NbOPO$_4$. The resulting ether yields are shown in **Figure 6b**, with selectivity data provided in **Table S5**. Increasing molar equivalents of H_2 showed an improvement in both ether yield and selectivity. Raising the WHSV to 2.3 h^{-1} decreased the yield of 4-BH yield and increased selectivity, while further raising the WHSV to 3.5 h^{-1} showed little change in either parameter.

Table 4. MFSP for producing 4-BH from wet waste derived butyric acid, with a breakdown of major cost contributions from the catalytic upgrading section of the process.

Case	MFSP ($/GGE)	Catalytic Upgrading Contribution	Catalyst Material & Reactor Contribution	H_2 Gas Usage Contribution
1	$4.56	$1.67	$0.48	$0.15
2	$4.36	$1.45	$0.44	$0.18
3	$4.32	$1.43	$0.42	$0.20
4	$4.52	$1.65	$0.41	$0.20
5	$4.61	$1.74	$0.37	$0.20

* Net MFSP penalties vs. the best case (Case 3) are due to changes in etherification yield and are therefore added into the catalytic upgrading contribution. Further details on the process model and assumptions can be found in the Supplemental Information.

The experimental results from the five process conditions above were then used to determine the impact on MFSP (**Figure 6c, Table 4**). Overall, increased yields of 4-BH corresponded to the minimal MFSP, which was observed with increasing H_2 equivalents and lower WHSV's. Expenses of additional H_2 usage were mitigated by employing a pressure-swing adsorption (PSA) system to recover and recycle H_2 after etherification. Accordingly, the net cost contribution of H_2 feed, recovery, and recycle did not change significantly between cases, contributing a consistent $0.15-0.20/GGE. Higher WHSV values were associated with lower catalyst and reactor costs; however, these savings were offset by the overall impact to 4-BH yield that resulted in the lowest MFSP at WHSV 1.2 h^{-1}. Overall, this analysis suggests that future catalyst material designs should focus on enabling high 4-BH single pass yields as the primary parameter for reducing process costs associated with reductive etherification.

Conclusion

The deployment of oxygenated ether diesel bioblendstocks requires significant de-risking of the technical production route and final fuel properties. Here, we outlined the development of a single-phase Pd/NbOPO$_4$ catalyst for the reductive

etherification of alcohols and ketones. Screening tests showed Pd/NbOPO$_4$ outperformed Pd/Nb$_2$O$_5$-PO$_4$ and Pd/TiO$_2$-PO$_4$ for producing 4-butoxyheptane under comparable reaction conditions in batch and in flow reactors. Continuous solvent-free catalytic testing demonstrated ether yields above 50% with minimal leaching of Pd and P observed during processing. Further, catalyst regeneration tests suggest an optimal Pd nanoparticle diameter above 10 nm. Several diesel-range branched ether molecules (C7-C15) were synthesized to characterize their fuel properties and demonstrate the broad substrate applicability of this catalyst for reductive etherification. Technoeconomic modelling determined that maximizing single-pass ether yields via higher hydrogen equivalents and lower weight hourly space velocity values outweigh the costs associated with increased catalyst material, reactor sizing, and hydrogen usage. Overall, these results highlight the potential of single-phase catalysts for reductive etherification and provide new insights to guide future catalyst material and process design efforts.

Conflicts of interest

G.R.H., N.A.H., X.H., and D.R.V. are inventors on a patent application submitted by the Alliance for Sustainable Energy on methods and materials for the production of ether bioblendstocks (US 62/847,700 filed 14 May 2019).

References

1. P. Fairley, *Nature*, 2011, **474**, S2-S5.
2. D. J. Gaspar, B. H. West, D. Ruddy, T. J. Wilke, E. Polikarpov, T. L. Alleman, A. George, E. Monroe, R. W. Davis, D. Vardon, A. D. Sutton, C. M. Moore, P. T. Benavides, J. Dunn, M. J. Biddy, S. B. Jones, M. D. Kass, J. A. Pihl, J. A. Pihl, M. M. Debusk, M. Sjoberg, J. Szybist, C. S. Sluder, G. Fioroni and W. J. Pitz, *Top Ten Blendstocks Derived From Biomass For Turbocharged Spark Ignition Engines: Bio-blendstocks With Potential for Highest Engine Efficiency*, United States, 2019.
3. B. M. Jenkins, L. L. Baxter, T. R. Miles and T. R. Miles, *Fuel Processing Technology*, 1998, **54**, 17-46.
4. X. Huo, N. A. Huq, J. Stunkel, N. S. Cleveland, A. K. Starace, A. E. Settle, A. M. York, R. S. Nelson, D. G. Brandner, L. Fouts, P. C. St. John, E. D. Christensen, J. Luecke, J. H. Mack, C. S. McEnally, P. A. Cherry, L. D. Pfefferle, T. J. Strathmann, D. Salvachúa, S. Kim, R. L. McCormick, G. T. Beckham and D. R. Vardon, *Green Chemistry*, 2019, **21**, 5813-5827.
5. G. Fioroni, L. Fouts, J. Luecke, D. Vardon, N. Huq, E. Christensen, X. Huo, T. Alleman, R. McCormick, M. Kass, E. Polikarpov, G. Kukkadapu and R. A. Whitesides, 2019.
6. D. D. Das, C. S. McEnally, T. A. Kwan, J. B. Zimmerman, W. J. Cannella, C. J. Mueller and L. D. Pfefferle, *Fuel*, 2017, **197**, 445-458.
7. C. S. McEnally and L. D. Pfefferle, *Environ Sci Technol*, 2011, **45**, 2498-2503.
8. B. M. Viswanathan, R. D. Raman, A. K. Rosentrater and H. B. Shanks, *Processes*, 2020, **8**.
9. T. J. Schwartz, B. H. Shanks and J. A. Dumesic, *Current Opinion in Biotechnology*, 2016, **38**, 54-62.
10. K. W. Harrison and B. G. Harvey, *Sustainable Energy & Fuels*, 2018, **2**, 367-371.
11. B. G. Harvey, W. W. Merriman and R. L. Quintana, *ChemSusChem*, 2016, **9**, 1814-1819.
12. B. Rozmysłowicz, J. H. Yeap, A. M. I. Elkhaiary, M. Talebi Amiri, R. L. Shahab, Y. M. Questell-Santiago, C. Xiros, B. P. Le Monnier, M. H. Studer and J. S. Luterbacher, *Green Chemistry*, 2019, **21**, 2801-2809.
13. N. A. Huq, X. Huo, G. R. Hafenstine, S. M. Tifft, J. Stunkel, E. D. Christensen, G. M. Fioroni, L. Fouts, R. L. McCormick, P. A. Cherry, C. S. McEnally, L. D. Pfefferle, M. R. Wiatrowski, P. T. Benavides, M. J. Biddy, R. M. Connatser, M. D. Kass, T. L. Alleman, P. C. St. John, S. Kim and D. R. Vardon, *Proceedings of the National Academy of Sciences*, 2019, **116**, 26421-26430.
14. J. Yan, L. Liang, Q. He, C. Li, F. Xu, J. Sun, E.-B. Goh, N. V. S. N. M. Konda, H. R. Beller, B. A. Simmons, T. R. Pray, V. S. Thompson, S. Singh and N. Sun, 2019, **12**, 4313-4322.
15. B. B. Bond-Watts, R. J. Bellerose and M. C. Y. Chang, *Nature Chemical Biology*, 2011, **7**, 222-227.
16. E. L. Kunkes, D. A. Simonetti, R. M. West, J. C. Serrano-Ruiz, C. A. Gärtner and J. A. Dumesic, *Science*, 2008, **322**, 417-421.
17. G.-J. t. Brink, I. W. C. E. Arends and R. A. Sheldon, *Science*, 2000, **287**, 1636-1639.
18. C. J. Wrasman, A. R. Riscoe, H. Lee and M. Cargnello, *ACS Catalysis*, 2020, **10**, 1716-1720.
19. C. J. Wrasman, A. Boubnov, A. R. Riscoe, A. S. Hoffman, S. R. Bare and M. Cargnello, *Journal of the American Chemical Society*, 2018, **140**, 12930-12939.
20. J. M. Lee, P. P. Upare, J. S. Chang, Y. K. Hwang, J. H. Lee, D. W. Hwang, D. Y. Hong, S. H. Lee, M. G. Jeong, Y. D. Kim and Y. U. Kwon, *ChemSusChem*, 2014, **7**, 2998-3001.
21. G. Strazzera, F. Battista, N. H. Garcia, N. Frison and D. Bolzonella, *Journal of Environmental Management*, 2018, **226**, 278-288.
22. O. Nagashima, S. Sato, R. Takahashi and T. Sodesawa, *Journal of Molecular Catalysis A: Chemical*, 2005, **227**, 231-239.
23. V. Pham, M. Holtzapple and M. El-Halwagi, *Journal of Industrial Microbiology & Biotechnology*, 2010, **37**, 1157-1168.
24. W. N. Chan, Z. Fu and M. T. Holtzapple, *Biomass and Bioenergy*, 2011, **35**, 4134-4144.
25. R. Pizzi, R.-J. Van Putten, H. Brust, S. Perathoner, G. Centi and J. Van Der Waal, *Catalysts*, 2015, **5**, 2244-2257.
26. X.-L. Li, K. Zhang, S.-Y. Chen, C. Li, F. Li, H.-J. Xu and Y. Fu, *Green Chemistry*, 2018, **20**, 1095-1105.
27. J. Wei, T. Wang, X. Cao, H. Liu, X. Tang, Y. Sun, X. Zeng, T. Lei, S. Liu and L. Lin, *Applied Catalysis B: Environmental*, 2019, **258**, 117793.
28. J. Wei, T. Wang, H. Liu, M. Li, X. Tang, Y. Sun, X. Zeng, L. Hu, T. Lei and L. Lin, *Energy Technology*, 2019, **7**, 1801071.
29. J. Rorrer, S. Pindi, F. D. Toste and A. T. Bell, *ChemSusChem*, 2018, **11**, 3104-3111.
30. N. M. Eagan, B. M. Moore, D. J. McClelland, A. M. Wittrig, E. Canales, M. P. Lanci and G. W. Huber, *Green Chemistry*, 2019, **21**, 3300-3318.
31. V. Bethmont, F. Fache and M. Lemaire, 1995, **36**, 4235-4236.
32. L. Gooßen and C. Linder, *Synlett*, 2006, **2006**, 3489-3491.
33. D. Jadhav, A. M. Grippo, S. Shylesh, A. A. Gokhale, J. Redshaw and A. T. Bell, *ChemSusChem*, 2017, DOI: 10.1002/cssc.201700427.
34. M. L. Tulchinsky and J. R. Briggs, *ACS Sustainble Chemistry & Engineering*, 2016, **4**, 4089-4093.
35. L. Maat, H. Bekkum, G. Luijkx, N. Huck and F. Rantwijk, *Heterocycles*, 2009, **77**.
36. V. Bethmont, C. Montassier and P. Marecot, *Journal of Molecular Catalysis A: Chemical*, 2000, **152**, 133-140.
37. Y. Fujii, H. Furugaki, E. Tamura, S. Yano and K. Kita, *Bulletin of the Chemical Society of Japan*, 2005, **78**, 456-463.
38. M. Balakrishnan, E. R. Sacia and A. T. Bell, 2012, **14**, 1626.
39. P. T. Anastas and J. C. Warner, *Green chemistry theory and practice*, Oxford [England] Oxford University Press, 2000.
40. R. Bringué, E. Ramírez, M. Iborra, J. Tejero and F. Cunill, 2014, **246**, 71-78.
41. M. Argyle and C. Bartholomew, *Catalysts*, 2015, **5**, 145-269.
42. V. D. Mvndale, H. S. Joglekar, A. Kalam and J. B. Joshi, *The Canadian Journal of Chemical Engineering*, 1991, **69**, 1149-1159.

43. H. Xiong, H. N. Pham and A. K. Datye, *Green Chemistry*, 2014, **16**, 4627-4643.

44. T. T. Pham, S. P. Crossley, T. Sooknoi, L. L. Lobban, D. E. Resasco and R. G. Mallinson, *Applied Catalysis A: General*, 2010, **379**, 135-140.

45. Y. Wang, Q. Cui, Y. Guan and P. Wu, *Green Chemistry*, 2018, **20**, 2110-2117.

46. Y. Long, Y. Wang, H. Wu, T. Xue, P. Wu and Y. Guan, *RSC Advances*, 2019, **9**, 25345-25350.

47. A. Garcia-Ortiz, K. S. Arias, M. J. Climent, A. Corma and S. Iborra, *ChemSusChem*, 2020, **13**, 707-714.

48. A. Badgett, E. Newes and A. Milbrandt, *Energy*, 2019, **176**, 224-234.

49. Y. Zhang, J. Wang, J. Ren, X. Liu, X. Li, Y. Xia, G. Lu and Y. Wang, *Catalysis Science & Technology*, 2012, **2**, 2485-2491.

50. Y. J. Pagán-Torres, J. M. R. Gallo, D. Wang, H. N. Pham, J. A. Libera, C. L. Marshall, J. W. Elam, A. K. Datye and J. A. Dumesic, *ACS Catalysis*, 2011, **1**, 1234-1245.

51. C. Hernández Mejía, J. H. den Otter, J. L. Weber and K. P. de Jong, *Applied Catalysis A: General*, 2017, **548**, 143-149.

52. R. Buitrago-Sierra, J. C. Serrano-Ruiz, F. Rodríguez-Reinoso, A. Sepúlveda-Escribano and J. A. Dumesic, *Green Chemistry*, 2012, **14**, 3318-3324.

53. L. Zhang, G. Wen, H. Liu, N. Wang and D. S. Su, *ChemCatChem*, 2014, **6**, 2600-2606.

54. M. Dahmen and W. Marquardt, *Energy & Fuels*, 2015, **29**, 5781-5801.

55. T. Kessler, E. R. Sacia, A. T. Bell and J. H. Mack, *Fuel*, 2017, **206**, 171-179.

56. P. C. St. John, P. Kairys, D. D. Das, C. S. McEnally, L. D. Pfefferle, D. J. Robichaud, M. R. Nimlos, B. T. Zigler, R. L. McCormick, T. D. Foust, Y. J. Bomble and S. Kim, *Energy & Fuels*, 2017, **31**, 9983-9990.

57. D. D. Das, P. C. St. John, C. S. McEnally, S. Kim and L. D. Pfefferle, *Combustion and Flame*, 2018, **190**, 349-364.

58. C. E. S. R. A. Mott, *Fuel*, 1940, **19**, 226-231, 242-251.

59. W. Boie, *Energietechnik*, 1953, **3**, 309-316.

60. W. G. Lloyd and D. A. Davenport, *Journal of Chemical Education*, 1980, **57**, 56.

61. L. Constantinou and R. Gani, *AIChE Journal*, 1994, **40**, 1697-1710.

62. L. D. Hughes, D. S. Palmer, F. Nigsch and J. B. O. Mitchell, *Journal of Chemical Information and Modeling*, 2008, **48**, 220-232.

63. R. W. Prugh, *Journal of Chemical Education*, 1973, **50**, A85.

64. R. M. Butler, G. M. Cooke, G. G. Lukk and B. G. Jameson, *Industrial & Engineering Chemistry*, 1956, **48**, 808-812.

65. A. E. Settle, N. S. Cleveland, C. A. Farberow, D. R. Conklin, X. Huo, A. A. Dameron, R. W. Tracy, R. Sarkar, E. J. Kautz, A. Devaraj, K. K. Ramasamy, M. J. Watson, A. M. York, R. M. Richards, K. A. Unocic, G. T. Beckham, M. B. Griffin, K. E. Hurst, E. C. D. Tan, S. T. Christensen and D. R. Vardon, *Joule*, 2019, **3**, 2219-2240.

66. ASTM, *ASTM D6571: Standard Specification for Biodiesel Fuel Blend Stock (B100) for Middle Distillate Fuels*

67. F. G. Baddour, L. Snowden-Swan, J. D. Super and K. M. Van Allsburg, *Organic Process Research & Development*, 2018, **22**, 1599-1605.

68. CatCost, a catalyst cost estimation tool, version 1.0.0; National Renewable Energy Lab: Golden, CO, USA, 2018; https://catcost.chemcatbio.org.

69. M. Kim, K.-Y. Kim, K. M. Lee, S. H. Youn, S.-M. Lee, H. M. Woo, M.-K. Oh and Y. Um, *Bioresource Technology*, 2016, **218**, 1208-1214.

70. E. M. Karp, R. M. Cywar, L. P. Manker, P. O. Saboe, C. T. Nimlos, D. Salvachúa, X. Wang, B. A. Black, M. L. Reed, W. E. Michener, N. A. Rorrer and G. T. Beckham, *ACS Sustainable Chemistry & Engineering*, 2018, **6**, 15273-15283.

71. X. Wang, D. Salvachúa, V. Sànchez i Nogué, W. E. Michener, A. D. Bratis, J. R. Dorgan and G. T. Beckham, *Biotechnology for Biofuels*, 2017, **10**, 200.

72. W. d. A. Cavalcante, R. C. Leitão, T. A. Gehring, L. T. Angenent and S. T. Santaella, *Process Biochemistry*, 2017, **54**, 106-119.